European Journal of Pharmaceutical Sciences 169 (2022) 106087

Contents lists available at ScienceDirect

European Journal of Pharmaceutical Sciences

journal homepage: www.elsevier.com/locate/ejps

Mechanistic study of dissolution enhancement by interactive mixtures of chitosan with meloxicam as model

Jana Brokešová [a], Michaela Slámová [b], Petr Zámostný [b], Martin Kuentz [c], Jakub Koktan [d], Lukáš Krejčík [d], Barbora Vraníková [a], Petra Svačinová [a], Zdenka Šklubalová [a,*]

[a] Department of Pharmaceutical Technology, Charles University, Faculty of Pharmacy, Akademika Heyrovského 1203/8, Hradec Králové 500 05, Czech Republic
[b] Department of Organic Technology, UCT Prague, Faculty of Chemical Technology, Technická 5, Dejvice, Prague 6 166 28, Czech Republic
[c] University of Applied Sciences and Arts Northwestern Switzerland, Institute of Pharma Technology, Hofackerstrasse 30, Muttenz CH-4132, Switzerland
[d] Zentiva, K.S., U Kabelovny 130, Prague 10 102 37, Czech Republic

ARTICLE INFO

Keywords:
BCS class II
Interactive mixture
Dissolution rate
Co-milling
Chitosan
Meloxicam

ABSTRACT

To enhance dissolution rate of meloxicam (MX), a poorly soluble model drug, a natural polysaccharide excipient chitosan (CH) is employed in this work as a carrier to prepare binary interactive mixtures by either mixing or co-milling techniques. The MX-CH mixtures of three different drug loads were characterized for morphological, granulometric, and thermal properties as well as drug crystallinity. The relative dissolution rate of MX was determined in phosphate buffer of pH 6.8 using the USP-4 apparatus; a significant increase in MX dissolution rate was observed for both mixed and co-milled mixtures comparing to the raw drug. Higher dissolution rate of MX was evidently connected to surface activation by mixing or milling, which was pronounced by the higher specific surface energy as detected by inverse gas chromatography. In addition to the particle size reduction, the carrier effect of the CH was confirmed for co-milling by linear regression between the MX maximum relative dissolution rate and the total surface area of the mixture ($R^2 = 0.863$). No MX amorphization or crystalline structure change were detected. The work of adhesion/cohesion ratio of 0.9 supports the existence of preferential adherence of MX to the coarse particles of CH to form stable interactive mixtures.

1. Introduction

Aqueous solubility and permeability through membranes, generally specified in the Biopharmaceutical Classification System (BCS) (Amidon et al., 1995; Lipinski, 2000; Tsume et al., 2014), are the key factors for orally administered drugs. Insufficient water solubility of a drug belonging to the BCS class II may cause poor absorption and limited bioavailability (Khan and Singh, 2016; Al-Kassas et al., 2017). An insufficient and slow absorption is particularly a problem if a fast therapeutic effect is targeted such as in case of analgesic, antihistamine, and vasodilating drugs. Therefore, many methods have been developed in order to improve the extent and rate of drug dissolution. Among others the preparation of lipid-based systems (Mu et al., 2013), cyclodextrin complexes (Dhakar et al., 2019), solid dispersions (Slámová et al., 2020), liquisolid systems (Vraníková et al., 2020), and cocrystals (Jirát et al., 2020) can be mentioned.

The drug dissolution rate can be often simply enhanced by particle size reduction, e.g. by milling, due to the increase in available surface area and the alteration in particle shape (Loh et al., 2015). Unfortunately, the higher surface free energy of the resultant fine powder can lead to higher cohesivity followed by particle aggregation. This paradoxically reduces the effective surface area by formation of agglomerates resulting in poor wetting in aqueous phase, which negatively impacts on dissolution rate (Capece et al., 2016; Varghese and Ghoroi, 2017; Saeki et al., 2019). The problem can be solved by the addition of a suitable excipient, for example a surfactant (Hamishehkar et al., 2014) or an inert pharmaceutical carrier, typically a hydrophilic polymer that enhances the wettability by conferring hydrophilicity to the hydrophobic drug particle surface (Liu et al., 2015; Loh et al., 2015; Hussain et al., 2018). Regarding the simplicity, efficiency and environmental acceptability, milling and particularly co-milling have been already used in the dissolution improvement of different drugs, for example ibuprofen (Varghese and Ghoroi, 2017), probucol (Li et al., 2017), carvedilol (Bolourchian et al., 2019) or dipfluzine (Yang et al., 2012) by using microcrystalline cellulose, copovidone, Soluplus®, povidone, sodium lauryl sulfate, and poloxamer 188 as additives.

* Corresponding author.
E-mail address: sklubalova@faf.cuni.cz (Z. Šklubalová).

https://doi.org/10.1016/j.ejps.2021.106087
Received 3 August 2021; Received in revised form 15 November 2021; Accepted 27 November 2021
Available online 2 December 2021

In a binary excipient-drug powder mixture, three different types of interactions between the particles of substances can be generated: drug - drug, excipient – excipient, and drug – excipient. The micronized drug substance generally possesses high surface energy leading to the strong cohesive drug - drug particle interactions. As a result, stable clusters or agglomerates are formed (Capece et al., 2015). In the presence of a suitable carrier, such agglomerates can be disrupted due to the mixing/co-milling procedure, the micronized drug particles can preferably adhere to the surface of excipient particles and the drug – excipient interactions can be achieved (Capece et al., 2016). Such newly formed interactive powder agglomerates represent the desirable arrangement of interactive mixtures with a drug (mono)layer on the carrier surface (Allahham and Maswadeh, 2014; Hagen et al., 2016; Školáková et al., 2019). The reduction of the drug aggregation level and thereby better drug wettability and faster dissolution together with improved mixture homogeneity and flow properties are the main advantages of interactive mixtures (Hagen et al., 2016; Lohrmann et al., 2007). The typical carrier excipients used in dosage forms include lactose, cellulose, povidone, mannitol or trehalose (Hooton et al., 2006; Lohrmann et al., 2007; Zhou and Morton, 2012; Liu et al., 2015). In this work, we used chitosan (CH), a polysaccharide copolymer comprising of glucosamine and N-acetylglucosamine, which is made by deacetylation of chitin. It is the nontoxic and non-irritant material and its basic nature makes it unique (Dutta et al., 2004). In pharmaceutical technology, CH has been used previously as a direct compression excipient (Badwan et al., 2015), a carrier in dry powder inhalers (Huang et al., 2018; Wang et al., 2018), to improve drugs stability (Li et al., 2019), and for targeted drug delivery (Garg et al., 2019). Chitosan or its derivatives were also used to enhance the dissolution rate of carvedilol (Shete et al., 2012) and amorphous MX by preparation of solid dispersions (Obaidat et al., 2017).

However, only if the adhesion force between an excipient and a drug is high enough, the interactive mixture is successfully formed and no agglomerates of the drug remain (Lohrmann et al., 2007). In summary, the balance of two main forces, firstly, the cohesion forces between the drug particles, secondly, the adhesion forces of the drug to the carrier particles, is necessary. The adhesive forces between the particles of naturally different substances are determined by properties of the surface which depend on their chemical nature as well as on the surface geometrical factors affecting the possible contact area (Hooton et al., 2006; Lohrmann et al., 2007; Kuncahyo and Choiri, 2015; Školáková et al., 2019). Different techniques were used to describe particle-particle interactions in a powder mixture. The amplitude and the range of interaction of the force–distance curve of the detachment force between two single particles or a sample surface can be analyzed by an atomic force microscope (Lohrmann et al., 2007; Bunker et al., 2011). Alternatively, the centrifuge technique can be used to study the relationship between the adhesion force and the magnitude of the centrifugal force needed to detach the particle from the surface of a carrier (Kulvanich and Stewart, 1987; Nguyen et al., 2010; Tran et al., 2021). However, the interparticle forces are generally related to the surface energy of the components in the mixture, which is not described by any of above-mentioned techniques. For this reason, the inverse gas chromatography (IGC) is another important technique as recently reported by Školáková et al. (2019). Another publication from Imperial College London (Karde et al., 2020) also used IGC to study interparticle structuring of a binary powder system. These two recent studies have different approaches but they both mark novelty in harnessing IGC to study interacting powder mixtures. This is especially attractive for mechanistic research using co-milling. Thus, applied mechanical energy activates the solid phase leading to amorphous-crystalline inter-conversion of a drug (Lin et al., 2010; Loh et al., 2015). The formulation principle of amorphous drug is well known to enhance apparent aqueous solubility and dissolution rate (Edueng et al., 2019; Slámová et al., 2020), but unfortunately, thermodynamically lower stability of amorphous bulk or surfaces makes this effect generally only time-limited (Bhende and Jadhav, 2012). Interesting are recent developments in the field of electrospinning that show much promise to enable successful amorphization, while achieving good kinetic stability, i.e. low tendency for recrystallization (Verreck et al., 2003; Yu et al., 2009; Nagy et al., 2012). However, any drug amorphization should consider the specific compound properties and it is mostly favourable for compounds with suitable glass-forming ability and/or by using special formulations with sufficient stabilizing excipients (Laitinen et al., 2013; Alhalaweh et al., 2015; Edueng et al., 2019; Bolourchian et al., 2019). Given these considerations, the effects on dissolution rate induced by mixing and milling have the best chance to be long lasting when they are facilitated primarily by a reduction of particle size and generation of stable interactive mixtures. By contrast, a marked amorphization induced by milling would be disadvantageous for such powder-based formulations with respect to market formulations that need sufficient shelf-life. The current literature appears to have a gap in targeting the optimum mechanisms as to how a stable dissolution increase can be achieved in powder mixtures and IGC would be interesting to use as novel analytics in the field of interacting pharmaceutical mixtures obtained by co-milling.

Therefore, this mechanistic work studies the improvement of the dissolution rate of a model, poorly soluble (BCS class II) drug meloxicam (MX) (Horváth et al., 2016; Freitas et al., 2017; Romani et al., 2018) by the preparation of binary interactive mixtures with CH as a carrier. The effect of CH on the dissolution rate of MX in mixtures prepared by mixing (physical mixtures) and co-milling techniques is investigated using three different MX-CH ratios and two milling times. The granulometric, thermal, crystal, and surface energy properties of mixtures as well as their stability are examined in detail.

2. Materials and methods

2.1. Materials

The model drug meloxicam (MX, Cadila Healthcare Ltd., India) was obtained as a gift sample (Zentiva, k. s., Czech Republic). Chitosan (CH, JBICHEM International trading, Co., Ltd., China) of 85% deacetylation grade was used as a carrier. Sodium hydroxide (Penta s.r.o., Czech Republic), potassium dihydrogen phosphate (Dr. Kulich Pharma, s.r.o., Czech Republic) and methanol - HPLC grade (Sigma-Aldrich, Czech Republic) as well as purified water were used for dissolution testing. Surface energy was determined using hexane (Sigma-Aldrich, Germany), heptane (Sigma-Aldrich, Germany), octane (Sigma-Aldrich, Germany), nonane (Sigma-Aldrich, USA), dichloromethane (Sigma-Aldrich, France), ethyl acetate (Sigma-Aldrich, USA), chloroform (Sigma-Aldrich, USA), 1,4-dioxane (Sigma-Aldrich, Germany) and toluene, ethanol, and acetone (SupraSolv®, Germany). All the probes were of GC quality.

Unless otherwise stated, measurements and manipulations were carried out at a controlled ambient temperature of 23.0 ± 1.0 °C and relative air humidity of 39.0 ± 12.0% (Hygrometer 608-H1, Testo, China).

2.2. Mixtures preparation

All powders were first sieved through a 500-μm sieve before their use. The binary mixed mixtures (physical mixtures, PM) of MX and CH were prepared in 1-1, 1-4 and 1-8 (w/w) ratios using a 3D shaker mixer (Turbula type T2F, WAB AG, Switzerland). A 130-mL glass container was filled with the required mass of substance weighted with a precision of 0.01 g (BOECO Balances BBI-32, $d = 0.1$ mg, Boeco + Co, Germany). A total load of 15 gs of sample was prepared. In all experimental runs, raw MX was placed between two layers of CH to ensure the homogeneity of mixture. The mixing conditions were set on 5 min at 34 rpm.

Subsequently, the binary co-milled mixtures (CM) were prepared utilizing a planetary ball mill (PM 100, Retsch, Germany) so that 2 g of each PM was co-milled for 15 min or 30 min at 300 rpm in a 25-mL

stainless steel milling jar using 100 stainless steel milling balls of 5 mm diameter.

2.3. Homogeneity assessment

Homogeneity assessment was performed to test the efficiency of the mixing process. Five samples of 13.4 ± 0.2 mg were randomly removed from the MX-CH 1–1 PM binary mixture. Samples were than dissolved in methanol in 25 ml volumetric flask using ultrasonic bath (WUC-A01H, Witeg Labortechnik GmbH, Germany) for 45 min. Aliquots (200 µl) removed from the sonicated solutions were diluted by phosphate buffer (pH 6.8) up to 2 ml. The absorbance of the samples was then detected by spectrophotometer Specord 205 (Analytic Jena AG, Germany) at wavelength of 363 nm in triplicate and the concentration of MX was calculated according to the calibration curve. Mean value ($n = 5$), standard deviation (SD) and coefficient of variation (CV) were evaluated. Resulting CV = 1.9% was assumed to be acceptable.

2.4. Particle size measurement

Particle size distribution was determined by Mastersizer 3000 (Malvern Instruments Ltd., United Kingdom) utilizing Mie theory of static light scattering. An adequate amount of dry powder sample was measured using Aero S unit (air dispersion mode) at an air pressure of 2.0 bar and a feed rate of 50% to control of the sample throughput and dispersion. The particle refractive indices for CH and MX were 1.52 (Azofeifa et al., 2012) and 1.72 (Bartos et al., 2018), respectively. The latter was used for the prepared binary mixtures as well. Particle sizes of x_{10} (µm), x_{50} (µm) and x_{90} (µm) and "span" value characterizing the width of particle volume size distribution were detected. The measurement was performed in triplicate for each sample.

2.5. Scanning electron microscopy (SEM)

Scanning electron microscope (Phenom Pro, Phenom-World B. V., Netherlands) with the Back-scattered Electron Detector (BSE) was used to generate images of micronized MX, CH, and their binary mixtures. The samples were carefully sprinkled onto a carbon conductive tape, an approximately 10-nm-thick gold layer was sputtered on the sample surface, and the acceleration voltage of 10 kV was applied.

2.6. Surface area analysis

The specific surface area S_{BET} (m^2/g) was measured using a Gemini VII 2390 (Micromeritics, USA). Before the measurement, the samples were preconditioned for 24 h at 80 °C under nitrogen gas using FlowPrep 060 (Micromeritics, USA) to remove atmospheric contaminants from the surface of the sample. A sample tube was then filled with approximately 0.8 g of the powder with a precision of 0.0001 g. Analysis of a sample consisted of multipoint measurements (7 points) over the range of 0.05–0.35 relative pressure (p/p_0) using nitrogen as adsorptive to form monolayer on a sample surface. Specific surface area was evaluated (Gemini VII Version 5.01 software) according to the BET (Brunauer-Emmett-Teller) theory. The measurement was performed in triplicate for each sample.

2.7. Dissolution study

Dissolution studies were carried out using the USP-4 flow-through cell apparatus Sotax CE-1 (Sotax AG, Switzerland) in an open-loop system (Slámová et al., 2021). A small holdup volume of the sample and fresh solvent contact are advantages of this apparatus to obtain dissolution rate profiles (Beyssac and Lavigne, 2005). The dissolution rate of MX was studied at a temperature 37.0 ± 0.5 °C. Raw MX (MX RAW), MX activated by mixing (MX blank PM) or milling for 15 min (MX blank CM 15), were used as blank samples. The samples were sieved through a 500-µm sieve and filled into a partially assembled dissolution powder cell. In order to keep a constant mass 5.0 mg of MX, the equivalent mass of sample ranging from 5 to 45 mg in regard to the higher content of CH excipient, was used. The dissolution medium, phosphate buffer of pH 6.8 (Obaidat and Obaidat, 2011; Han and Choi, 2007), flow rate was set to 22 mL/min by a piston pump Sotax CY 1–50 (Sotax AG, Switzerland).

The exiting solution was collected manually for 15 min; the time interval was 20 s in the first three minutes following with the 1 min intervals for the next 12 min. The concentration of drug was detected spectroscopically as described above.

The relative amount of released drug m_{rel}, showing the relative amount of dissolved drug in%, and the relative dissolution rate r_{rel} (min^{-1}), considering the effect of mass of the drug in the sample, were calculated using Eqs. (1) and (2), respectively, where c is the measured concentration at the outlet of the dissolution cell (mg/L), Q is the media flow rate (L/s), t is the sampling interval (s) and m_{MX} is the total mass of the drug in the sample (mg).

$$m_{rel} = \frac{\sum c \times Q \times t}{m_{MX}} \times 100 \quad (1)$$

$$r_{rel} = \frac{c \times Q}{m_{MX}} \quad (2)$$

The dissolution experiments were carried out in triplicate. The mean values of m_{rel} (%) and r_{rel} (min^{-1}) and the standard deviations (SD) were calculated.

2.8. Surface energy analysis (SEA)

Surface energy was determined using IGC Surface energy analyzer (IGS/SEA, Surface Measurement Systems, Ltd., United Kingdom) equipped with Zero Air Generator GC 1500 (LNI Schmidlin SA, Switzerland) and Hydrogen Generator PG H2 (Schmidlin-DBS AG, Switzerland) at target column temperature 30 °C and 0% of relative humidity (RH). As a carrier gas, helium with the flow rate 10 mL/min was used. Dead volume was determined using methane as a reference gas at the beginning and the end of each measurement. The injector manifold was heated at 60 °C and the FID detector at 180 °C. A 3-mm glass column plugged by a small piece of silanized glass wool (Sigma-Aldrich, USA) was loaded with the appropriate mass of compacted powder sample (50–250 mg). The column was plugged with glass wool again at upper position and placed into the device. Prior to the analysis, the sample was preconditioned for 120 min.

For determining the dispersive surface energy, non-polar probes (hexane, heptane, octane, nonane) were used. Polar probes dichloromethane, ethyl acetate, chloroform, toluene, ethanol, acetone, and 1,4-dioxane were used for determining the specific surface energy. The constant fractional sample surface coverage was 5% (targeting infinite dilution conditions). Each measurement was performed in triplicate. The retention time of each injection was taken from maximum peak height.

Surface free energy as well as work of cohesion were calculated according to Schultz approach (Schultz et al., 1987); dispersive γ^D and specific γ^{SP} component of the surface energy were determined from a plot of $RT\ln V_N$ versus $a(\gamma_L^D)^{1/2}$. γ^D was calculated from the slope of the n-alkane line and γ^{SP} was estimated from the vertical distance between the alkane line and the polar probe. The values of the dispersive surface energy with regression coefficient $R^2 > 0.994$ were accepted. Acid and base number were evaluated according to Gutmann approach (Panayiotou et al., 2017). The ratio of basic to the acidic parameter K_B/K_A was calculated to determine the acid/base properties of the surface.

2.9. Thermal gravimetric analysis (TGA)

Thermal properties and stability of samples were measured by a TGA Q500 (TA Instruments, USA). The thermogravimetric analysis was

Table 1
Granulometric and surface characteristics of meloxicam (MX), chitosan (CH) and their prepared binary physical (PM) and co-milled (CM) mixtures.

Sample	x_{10} (μm)	x_{50} (μm)	x_{90} (μm)	span	S_{BET} (m^2/g)	K_B/K_A
MX RAW	1.1	3.7	8.2	1.94	2.1 ± 0.08	0.74
MX blank PM	1.3	4.2	9.1	1.86	1.9 ± 0.03	0.72
MX blank CM 15	1.5	10.4	230.0	21.97	5.8 ± 0.04	0.79
CH	20.1	61.2	158.0	2.26	0.8 ± 0.02	1.57
MX-CH 1–1 PM	3.6	43.6	146.0	3.27	1.4 ± 0.06	0.86
MX-CH 1–1 CM 15	4.8	47.5	139.0	2.82	3.7 ± 0.17	0.98
MX-CH 1–1 CM 30	4.6	38.6	121.0	3.02	5.3 ± 0.01	1.04
MX-CH 1–4 PM	9.1	54.6	151.0	2.60	1.0 ± 0.15	1.34
MX-CH 1–4 CM 15	11.0	49.6	141.0	2.62	2.8 ± 0.05	1.14
MX-CH 1–4 CM 30	9.5	42.5	121.0	2.61	4.2 ± 0.17	1.13
MX-CH 1–8 PM	13.8	57.4	153.0	2.42	1.0 ± 0.06	1.34
MX-CH 1–8 CM 15	12.9	50.7	139.0	2.48	2.3 ± 0.07	1.23
MX-CH 1–8 CM 30	11.1	43.6	123.0	2.56	2.9 ± 0.14	1.18

carried out in a temperature range of 25–900 °C at a heating rate of 10.00 °C/min under air purge utilizing platinum pan type.

2.10. Modulated differential scanning calorimetry (MDSC)

Glass transition temperature T_g (°C), melting point T_{mp} (°C) and heat of fusion ΔH (J/g) of all samples were evaluated using modulated differential scanning calorimetry (Discovery DSC, TA Instruments, USA). The appropriate mass of sample (a precision 0.001 mg) in a standard aluminum pan was scanned under nitrogen atmosphere (50 mL/min) at the temperature range of 0 °C to 270 °C with 5 min of stabilization at the beginning of the measurement. The heating rate of 5 °C/min, 60 s of modulation period and amplitude of 0.8 °C were used.

2.11. Powder X-ray diffraction (XRPD)

XRPD analysis was carried out using laboratory XPERT PRO MPD (PANalytical, Netherlands) diffractometer with CuKα (λ = 1.542 Å) radiation to determine the crystallinity of MX and CH. The generator operated at excitation voltage 45 kV and anodic current 40 mA. For the samples placed on a zero-background silica sample holder, the following scan parameters were utilized: scan type – gonio, measurement range 2–40° 2θ, step size 0.02° 2θ and time per step 200 s.

2.12. Stability studies

A stability study was performed in a stability chamber Memmert HCP 108 (Memmert GmbH, Germany) at temperature of 40 °C and 75% relative air humidity. The properties of two selected mixtures (MX-CH 1–8 PM, MX-CH 1–8 CM 30) were analyzed immediately after preparation and after 1 month (coded MX-CH 1–8 PM STAB, MX-CH 1–8 CM 30 STAB).

2.13. Statistical analysis

Experimental data were processed in MS Excel. The analysis of variance (ANOVA) at a significance level α of 0.05 was used to evaluate the influence of the preparation method, the drug/carrier ratio and the milling time. Additionally, post hoc Tukey's multiple comparisons test was performed using GraphPad Prism 9.2.0 (GraphPad Software, Inc., USA).

3. Results and discussion

Different technological strategies to enhance drug dissolution have been introduced to cope with poor aqueous solubility of BCS II drugs as described above. To explain mechanistic aspects, mixtures of the model lipophilic, and acidic drug MX (Freitas et al., 2017) were prepared with CH as a carrier. A simple mixing or alternative co-milling was selected in order to produce formulations having a different kind of drug-carrier interactive units. The mechanisms of interactive mixtures formation, their sensitivity to the preparation process, and the formulation effects on MX drug release were investigated by surface energy analysis and dissolution experiments.

3.1. Particle size and morphology

The size and shape of particles influence powder dissolution rate and play a critical role in the contact between the drug and a dissolution medium as well as between a drug and a carrier. The particle size and size distribution of substances were determined using the static light scattering method. Particle size characteristics for all substances used and the prepared mixtures are summarized in Table 1. The micronized particles of MX (RAW) are characterized with the median size of 3.7 μm, the span 1.94 and the specific surface area (S_{BET}) of 2.1 m^2/g. In Fig. 1a, the micronized particles of RAW MX forming agglomerates are shown. Contrary, particles of CH have the median particle size of 61.2 μm, wider particle size distribution (span 2.26) and low specific surface area of 0.8 m^2/g. The larger, platelet particles of CH are illustrated in Fig. 1b.

In order to discuss and compare the effects of the ratio between MX and CH, the method used, and the time of co-milling on the dissolution rate of MX, granulometric characteristics of the RAW MX in Table 1 were compared with those obtained by activation (without any carrier or other excipient) in a mixer (MX blank PM) or by milling in a ball mill for 15 min (MX blank CM 15). Although only MX substance without any excipient was processed by milling, the sample was coded "CM" to keep consistent coding with the other milled samples.

As can be seen, the median particle size x_{50} increased from 3.7 μm for the original substance (RAW) to 4.2 μm (PM) and, paradoxically, to 10.4 μm for MX blank CM 15. Milling for 15 min (MX blank CM 15) also significantly increased the portion of larger particles (x_{90} = 230 μm), which resulted in increased span value contrary to simple mixing in the 3D mixer (MX blank PM in Table 1). This is the result of *in situ* formed agglomerates of the fine drug particles. Thus, the mixing or milling the drug particles had no significant effect towards particle size reduction, but the particles still underwent a substantial structural change when milled. The almost 3-fold increase in S_{BET} observed between MX RAW and MX blank CM 15 was an evidence the formed agglomerates that comprise primary particles of reduced size and/or more rugged surface compared to original drug. The sample MX blank CM 30 was not included for subsequent characterization as serious sticking and sample hardening was observed by the milling for 30 min, which is considered a natural progress of the agglomeration as observed even for a shorter milling time. It is evident that processing the drug without any excipient produces some unexpected issues, but this way the drug particles obtain also new structural features, which can be beneficial for improving drug release from co-milled systems.

In Table 1, the granulometric properties of binary mixtures prepared either by simple mixing (PM) or co-milling (CM) in different drug/carrier ratios (MX-CH 1–1, MX-CH 1–4, MX-CH 1–8) are specified. The coding for milling respects 15 or 30 (CM 15 or CM 30, respectively) minutes procedure, as well. The median particle size 43.6 μm, 54.6 μm, and 57.4 μm of PM mixtures increases with the increase in content of CH,

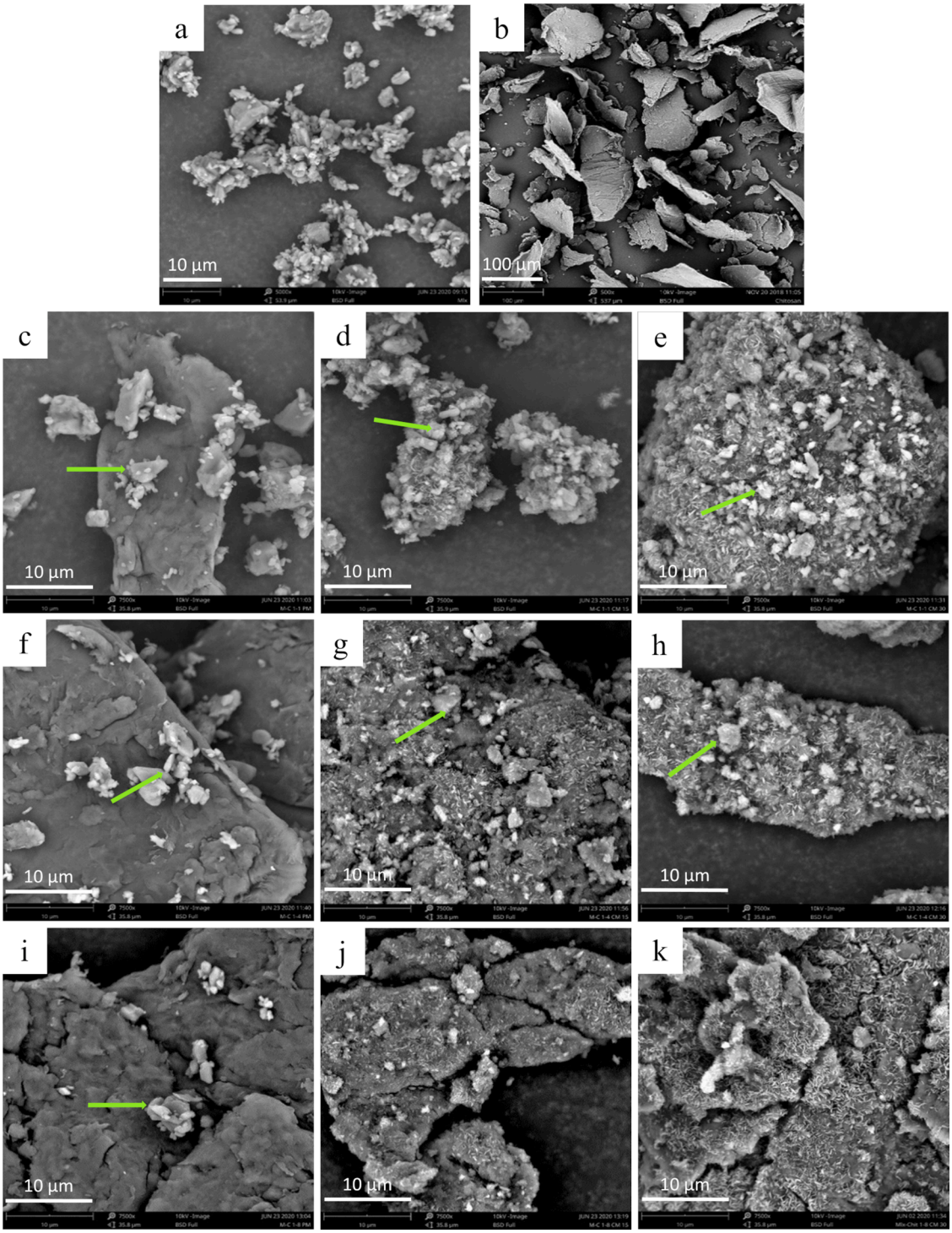

Fig. 1. SEM micrographs of raw substances (a Meloxicam (magnification 5000x), b Chitosan (magnification 500x)) and their physical and co-milled binary mixtures (c MX-CH 1–1 PM, d MX-CH 1–1 CM 15, e MX-CH 1–1 CM 30, f MX-CH 1–4 PM, g MX-CH 1–4 CM 15, h MX-CH 1–4 CM 30, i MX-CH 1–8 PM, j MX-CH 1–8 CM 15, k MX-CH 1–8 CM 30 (magnification 7 500x)). The inserted arrows show the meloxicam particle agglomerates.

which is the result of larger CH particles. The S_{BET} for co-milled samples follows a linear trend in relation to MX content. For example, all the samples milled for 15 min exhibit $S_{BET} = 3.84m_{MX} + 1.91$ m^2/g ($R^2 = 0.995$). It means the particle character was not likely affected by the dilution ratio MX-CH.

Similarly, the slight increase in median size for CM mixtures milled for 15 min was observed proportionally to the increase in CH content but the reduction in x_{90} (µm) and span values illustrate the general decrease in particle size due to the comminution. The effect of longer milling time is more visible when mixtures with the same MX-CH ratio are compared. For example, the median particle size of MX-CH 1–8 CM 15 was reduced from 50.7 µm to 43.6 µm for MX-CH 1–8 CM 30, whereas an increase in specific surface area from 2.3 to 2.9 m^2/g was observed. The span values of co-milled mixtures were similar regardless the milling time. However, the particle size reduction together with the higher specific surface area are in general beneficial for a faster drug dissolution (Beyssac and Lavigne, 2005; Rasenack and Müller, 2004).

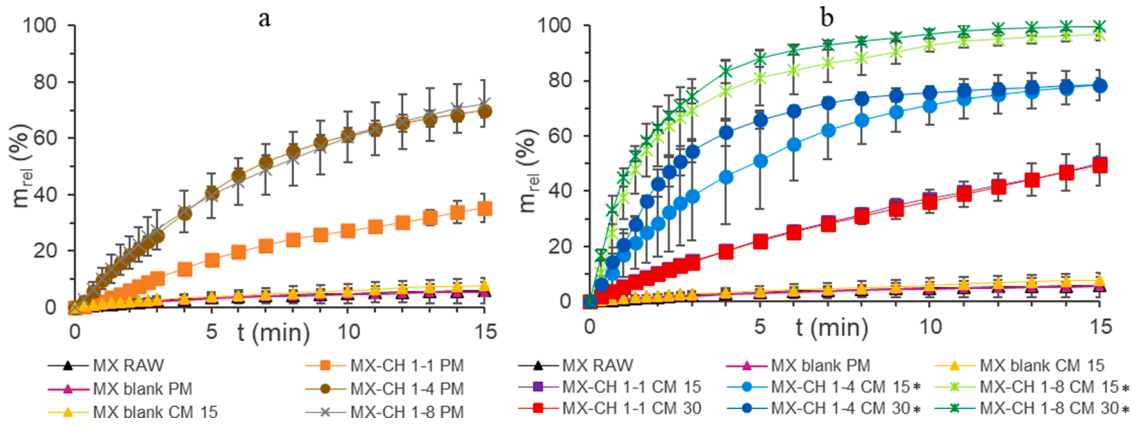

Fig. 2. Relative amount of released meloxicam after 15 min (a Meloxicam blank samples and mixed physical MX-CH binary mixtures, b Meloxicam blank samples and co-milled MX-CH binary mixtures). Asterisks in the legend indicate a significant result according to Tukey's post hoc test. Details are explained in text.

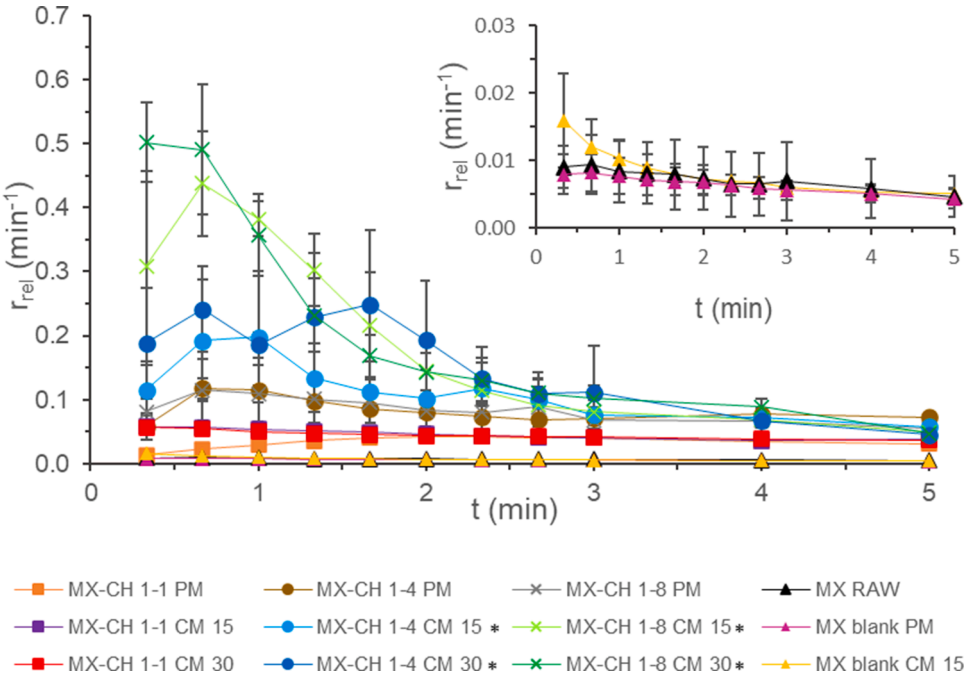

Fig. 3. Comparison of relative dissolution rates of meloxicam blank samples and MX-CH binary mixtures; the inserted graph shows meloxicam blank samples. Asterisks in the legend indicate a significant result according to Tukey's post hoc test. Details are given in the text.

3.2. Dissolution studies

The dissolution rate of MX was studied by a flow-through powder dissolution cell in an open-loop system (Slámová et al., 2021; Beyssac and Lavigne, 2005). The relative amount of released drug m_{rel} (in%) and the relative dissolution rate r_{rel} (min^{-1}) were determined by Eqs. (1) and 2, respectively.

3.2.1. MX dissolution rate

Firstly, the m_{rel} of raw meloxicam (MX RAW) was evaluated. As illustrated in Fig. 2a, it reaches only approximately 6% of the total drug content in a sample after 15 min of dissolution test. The poor dissolution of the micronized drug particles (x_{50} = 3.7 μm) was caused principally by the cohesiveness and tendency to form agglomerates (Fig. 1a) which in turn reduced wetting by the dissolution medium (Loh et al., 2015; Varghese and Ghoroi, 2017). Similar values of m_{rel} (Fig. 2a) were observed also for MX blank PM activated by mixing and by milling for 15 min (MX blank CM 15).

In Fig. 3, the comparison of relative dissolution rates r_{rel} (min^{-1}) of MX RAW and MX blank PM is depicted as an inserted graph. The relative dissolution rates were similarly low (r_{rel} < 0.01 min^{-1}) showing no activation by simple mixing. The higher r_{rel} 0.01–0.02 min^{-1} of MX blank CM 15 in the first 60 s can be explained as the result of the first contact between the medium and available partially size-reduced drug particles. This effect was only temporal, and we concluded that even milling of drug particles did not lead to the dissolution process activation. All pure MX samples were therefore assumed to be the blank MX samples.

3.2.2. The effect of mixing with CH on MX dissolution rate

Mixing with a suitable carrier belongs to the simplest methods used to increase drug dissolution rate in pharmaceutical technology and different fillers or surfactants are used (e.g. Pilcer et al., 2012, Loh et al., 2015, Marinko and Zámostný, 2020). The preparation of an interactive mixture represents here the common target. The binary interactive MX-CH mixtures obtained in this study by mixing (coded PM) are

illustrated in Fig. 1c,f,i according to the three ratios used: 1–1, 1–4, and 1–8, respectively. Although some of the MX particles adhere to the CH surface, nevertheless, there is a relatively high part of those remaining agglomerated and non-attached.

The results of the dissolution tests for the physical interactive mixtures are shown in Figs. 2a and 3. When compared with the blank MX samples, the increase in m_{rel} as well as in r_{rel} was observed in all samples by using CH as a carrier. However, the positive effect on MX dissolution rate was influenced by the different drug/excipient ratio used; the mixtures with the higher portion of CH provided a higher relative amount of dissolved drug.

The percentage amount of MX (Fig. 2a) released from MX-CH 1–1 mixture revealed an increase to approximately 35% of the total drug content within 15 min, while the 1–4 and 1–8 ratio mixtures achieved even as much as 70%. This effect is better illustrated when looking at the relative dissolution rate (Fig. 3). The r_{rel} values of MX-CH 1–1 mixture raised slowly, the maximum relative dissolution rate r_{MAX} 0.04 min^{-1} was achieved within two minutes and it remained unchanged within 15 min of the dissolution test. Similar profiles, but the higher r_{MAX} of MX were observed for the MX-CH 1–4 and MX-CH 1–8 mixtures (0.12 min^{-1} and 0.11 min^{-1}, respectively) within the first minute while it has to be reminded that the amount of drug in all tested samples was identical.

The results confirmed that mixing with CH brings beneficial improvement in dissolution rate of MX; the concentration dependent CH effect was observed with the higher efficiency when higher portion of CH was used in the binary mixtures. The shear forces produced during mixing resulted in a partial desagglomeration and redistribution of the micronized MX on the CH surface without changing their particle size.

3.2.3. The effect of co-milling with CH on MX dissolution rate

Milling or co-milling with a suitable carrier are relatively easy methods to increase dissolution rate of poorly soluble drugs simply by particle size reduction and increase in surface available for dissolution (Yang et al., 2012; Varghese and Ghoroi, 2017; Bolourchian et al., 2019). As commented above for MX (MX blank CM 15, Table 1), the comminution of such a hydrophobic drug substance, particularly when no liquid medium or stabilizer is used, can unfortunately lead to particle agglomeration, which reduces surface area available for solvent wetting (Loh et al., 2015). Such a problem can be overcome by the addition of a suitable excipient allowing for the preparation of interactive mixtures (Li et al., 2017). By co-milling of MX in the presence of CH for 15 or 30 min, binary MX-CH mixtures (coded CM and having different ratios as mentioned above) were prepared. Figs. 1d,e,g,h,j,k illustrate the fine drug particles adhering to the surface of coarse CH particles. As described above for mixing, the same MX-CH ratio dependence was observed. While the micronized drug particles were homogeneously spread onto CH particle surface in the MX-CH 1–8 CM 30 sample (Fig. 1k), occasional agglomerates were visible in the MX-CH 1–4 CM 30 sample (Fig. 1h) and even more in the MX-CH 1–1 CM 30 sample (Fig. 1e).

In Fig. 2b, the relative amount of drug m_{rel} released from co-milled mixtures is shown. The significantly higher m_{rel} was detected for all CM mixtures compared with the milled drug (MX blank CM 15, Fig. 2a). Indeed, the higher portion of CH, the higher m_{rel} was noted with the best result achieved with MX-CH 1–8 mixtures ($m_{rel} > 95\%$).

Considering the same drug mass in the sample, slightly higher effect on the r_{rel} was detected for MX-CH 1–1 CM 15 and MX-CH 1–1 CM 30 mixtures (Fig. 3) when compared with MX blank CM 15. Contrary, the relative dissolution rates r_{rel} of MX in MX-CH 1–4 CM 15, MX-CH 1–4 CM 30, MX-CH 1–8 CM 15, and MX-CH 1–8 CM 30 mixtures were higher. The co-milling effect was studied also by an ANOVA and Tukey's post hoc test at $\alpha = 0.05$. As a result, a significant effect ($p < 0.01$) was confirmed when comparing the m_{rel} (%), r_{rel} (min^{-1}), and r_{MAX} (min^{-1}) of MX RAW, MX blank PM, and MX blank CM 15 with corresponding values of MX-CH 1–4 CM 15, MX-CH 1–4 CM 30, MX-CH 1–8 CM 15, and MX-CH 1–8 CM 30. Although the differences in effect of milling time

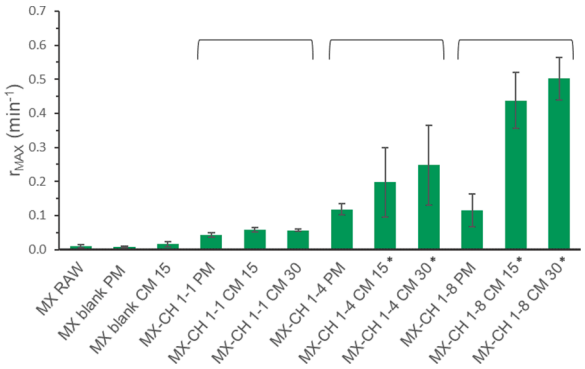

Fig. 4. Comparison of maximum relative dissolution rates r_{MAX} (min^{-1}) of meloxicam. The results are shown in groups according to the drug/excipient ratio. Asterisks in the legend indicate a significant result according to Tukey's post hoc test.

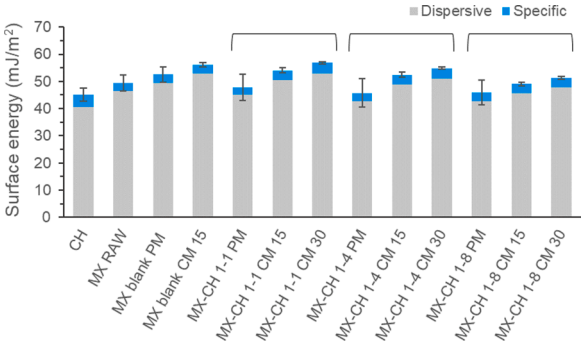

Fig. 5. Surface energy characterization of meloxicam, chitosan and physical mixed and co-milled MX-CH binary mixtures (the results are shown in groups according to the drug/excipient ratio).

were insignificant (ANOVA, $p \leq 0.05$), the higher r_{rel} was observed for 30 CM sample within the first minute. This is in agreement with the common observation that longer milling time improves typically the dissolution profile (Hussain et al., 2018; Loh et al., 2015).

Indeed, the r_{rel} reached a maximum at the beginning of the dissolution process due to the first contact of dissolution medium with the micronized particles located on the CH particle surface. Although the r_{rel} decreased later, the higher values were observed (Fig. 3) for interactive CM mixtures at the beginning of dissolution than that detected with the blank MX milled sample (MX blank CM 15).

Based on the results of dissolution studies, the following findings can be summarized: (i) mixing as well as co-milling with CH enhanced the dissolution rate of MX significantly (ANOVA, $p < 1.05 \times 10^{-10}$ at $\alpha = 0.05$); (ii) a noticeably better effect of co-milling was detected; (iii) the effect of CH on the MX dissolution rate was directly ratio dependent. The benefit of CH use in the preparation of MX-CH interactive mixtures is clearly visible in Fig. 4 where maximum relative dissolution rates r_{MAX} (min^{-1}) of all tested MX samples are compared.

3.3. Surface energy studies

Two key factors influence homogeneity of a powder mixture: segregation and agglomeration, both dependent on the interparticle interaction forces (Lai et al., 1981; Lohrmann et al., 2007) and both affecting the quality of the final product. To obtain uniform and stable interactive mixtures, sufficiently strong adhesion forces between the drug and carrier particles are crucial. Adhesion forces depend on the interfacial energy between two surfaces in the contact (Podczeck et al., 1997) and can be determined by inverse gas chromatography (IGC)

(Školáková et al., 2019). In order to study the surface energy of powder substances used, CH and MX and their interactive mixtures, were analyzed by IGC/SEA in terms of both dispersive and specific energy components. The results are shown in Fig. 5.

For fine, dry, uncharged powders, Van der Waals interaction forces expressed by the nonpolar dispersive component of surface energy dominate (De Kruif et al., 2013; Capece et al., 2015). By using of n-alkanes series, the dispersive component of surface energy was estimated. The γ^D value of MX RAW 46.5 mJ/m^2 was higher compared to that of CH (40.6 mJ/m^2) showing its nonpolar nature. The surface activation and the increase in γ^D due to the process-induced local disorders was expected for mixtures. This is generally the reason for more intensive contact with a dissolution liquid medium and the increase in dissolution rate (Varghese and Ghoroi, 2017). For the blank samples MX blank PM and MX blank CM 15, the γ^D increased due to mixing and milling to 49.5 and 52.8 mJ/m^2, respectively, which reflects higher-energy places occurring on the sample surface. As a result, r_{max} increased almost twice for MX blank CM 15 (0.0159 min^{-1}) in comparison to MX RAW (0.0093 min^{-1}). This can be attributed firstly to the change in surface structure and roughness (the local disruption of crystal structure), and secondly, to a partial surface amorphization.

The specific components of surface energy (γ^{SP}) were estimated using seven polar probes as these can allow to detect polar groups based on Lewis acid-base interactions (De Kruif et al., 2013). The higher specific surface energy of CH (4.5 mJ/m^2) compared with MX (2.9 mJ/m^2) confirmed its more polar nature and can be mostly attributed to the polar surface -OH groups of the polysaccharide. Principally, the hydrophilic nature of a carrier makes the drug dissolution in interactive mixtures easier and faster (Varghese and Ghoroi, 2017). In agreement, the largest specific surface energy was always detected in MX-CH 1–8 ratio in comparison with other MX-CH mixtures (Fig. 5).

In a MX-CH 1–8 ratio, the best effect of CH on MX dissolution rate was observed as discussed in Sections 3.2.2 and 3.2.3. Comparing the close γ^D values of mixed (MX-CH 1–8 PM) and milled (MX-CH 1–8 CM 15, MX-CH 1–8 CM 30) interactive mixtures (Fig. 5), it seems evident that albeit there are effects of surface disorder as mentioned above, it is to a great extent the hydrophilic nature of the used carrier excipient in the interacting mixture that contributed to the high observed maximum dissolution rates of 0.1149 min^{-1}, 0.4375 min^{-1}, and 0.5020 min^{-1}, respectively. By providing hydrophilicity as a carrier to the hydrophobic drug particle surfaces, the added excipient enhances the wettability and dissolution rate of the poorly water-soluble drug (Loh et al., 2015).

To describe the surface properties in more details, the constants of acidity K_A and basicity K_B were calculated using the donor (basicity) and acceptor (acidity) number of the Gutmann approach (Panayiotou et al., 2017). The empirical ratio of Lewis basic to acid parameter (K_B /K_A) reveals the nature of the surface in terms of electron pair donor to acceptor tendency (Varghese and Ghoroi, 2017); when $K_B/K_A > 1$, the electron donor ability prevails over the electron acceptor, while opposite is true for $K_B/K_A < 1$. The results are summarized in Table 1. The ratio 0.74 of raw MX increases after mixing and co-milling with CH meaning the increase in basicity of the prepared mixtures. This is attributed to formation of new interactions between drug and carrier, which reduced the acidity of MX .

In a powder mixture, the interactions between particles of individual substances are important (Capece et al., 2015). In our binary mixtures, this includes three different types of interactions: MX-MX, CH—CH, and MX-CH. Generally, micronized drug can show strong cohesive behavior, thereby forming clusters or agglomerates. In interactive mixtures, adhesion between fine drug particles and a carrier having high-energy sites on the surface is necessary for stability (Capece et al., 2016). Assuming that each individual substance contributes to the different energy components in the mixture based on a given mass fraction, the preferential interactions can be estimated from the surface parameters as recently shown by Školáková et al. (2019).

In order to predict the tendency of the micronized substance (MX) to create preferential bonds to the coarse particles of carrier (CH), the work of adhesion and the work of cohesion were estimated based on the measured surface energy using Fowkes theory (Fowkes, 1964) following with expression of the W_{adh}/W_{coh} ratio. The results are shown in Table 2.

Table 2
Values of work of adhesion (W_{adh}), work of cohesion (W_{coh}), their dispersive (W_{adh}^D, W_{coh}^D) and specific components (W_{adh}^{SP}, W_{coh}^{SP}).

Parameter (mJ/m^2)	Sample MX RAW	CH	MX-CH
W_{coh}^D	92.9	81.2	
W_{coh}^{SP}	5.8	8.9	
W_{coh}	98.7	90.1	
W_{adh}^D			85.7
W_{adh}^{SP}			7.1
W_{adh}			92.9

While the high work of cohesion shows high tendency of agglomeration between particles of the same substance, the high work of adhesion indicates the tendency of particle to adhere to the particle of another type. Higher adhesion properties can also prevent segregation during e.g. mixing with the other additives. In our mixtures, the W_{adh}/W_{coh} ratio calculated from the adhesion work of MX-CH (92.9 mJ/m^2) and the cohesion work of MX RAW (98.7 mJ/m^2) was 0.9 indicating the balance of forces. This finding confirmed the ability of CH to form the stable interactive mixture with MX.

3.4. Mechanism of CH action

Comparing finally the efficiency of CH addition on the MX dissolution rate, however, the higher effect of co-milling over mixing was detected. This can be firstly attributed to the drug micronization as well as the local surface disorder associated with the surface activation, and secondly, to the suppression of drug-drug particle agglomeration because of their proper distribution onto the carrier surface. Such drug particles are better accessible for the dissolution medium and their dissolution becomes enhanced which was directly expressed by the higher MX r_{MAX} (min^{-1}). As the design of experiments was based on maintaining the same mass of drug in each dissolution experiment (m_{MX} = 5 mg = 0.005 g) and total amount of the sample changed from 5 to 45 mg accordingly, two boundary hypotheses would be suggested to make final decision about the CH effect (considering also the MX-CH ratio has no significant effect on the character of MX particles in co-milling mixture as discussed above in 3.1).

The first one assumes no significant effect of the CH carrier. Under such circumstance, the dissolution rate should be increased only due to the milling effect and proportional to the surface area of the drug mass fraction m_{MX} which is equivalent to specific surface area of the sample $S_{BET} \times m_{MX}$. No relationship supporting such hypothesis was detected when plotting $S_{BET} \times m_{MX}$ against the MX r_{MAX} (Fig. 6a).

The second hypothesis assumes a so called “complete carrier effect” of the CH particle, so that virtually all of the surface area is formed by the drug layer spread homogenously out on its surface. The dissolution rate hence should be proportional to the total surface area of the mixture and the relative mass fraction of MX (w_{MX}) in the mixture, i.e. $S_{TOTAL} = S_{BET}/w_{MX} \times m_{MX}$. The second hypothesis was indeed supported by a linear relationship (Fig. 6b) with the MX r_{MAX} to yield a coefficient of determination $R^2 = 0.863$:

$$r_{MAX} = 3.7917 \times S_{TOTAL} - 0.049 \quad (3)$$

Based on the obtained results, it can be therefore concluded that CH is able to act as a suitable carrier in the co-milling process, so that the specific surface area of the mixture as well as the total amount of the mixture (i.e. the total surface) are the controlling parameters of the dissolution rate. This is the major effect observed, confirmed by a high correlation ($R^2 = 0.992$) between the total surface energy of the system ($\gamma_{TOTAL} = S_{TOTAL} \times (\gamma^D + \gamma^{SP})$) and S_{TOTAL}. It demonstrates that the total

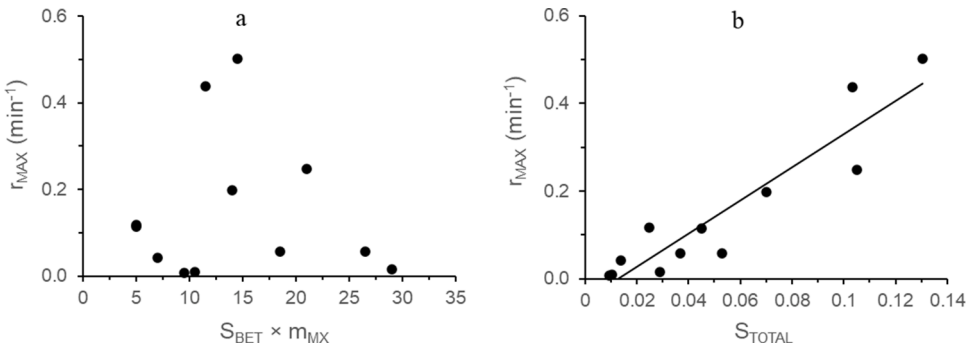

Fig. 6. Explanation of chitosan effect: a correlation between MX dissolution rate r_{MAX} (min^{-1}) and specific surface area of the sample $S_{BET} \times m_{MX}$; b correlation between MX dissolution rate r_{MAX} (min^{-1}) and S_{TOTAL} (m^2). Details are given in the text.

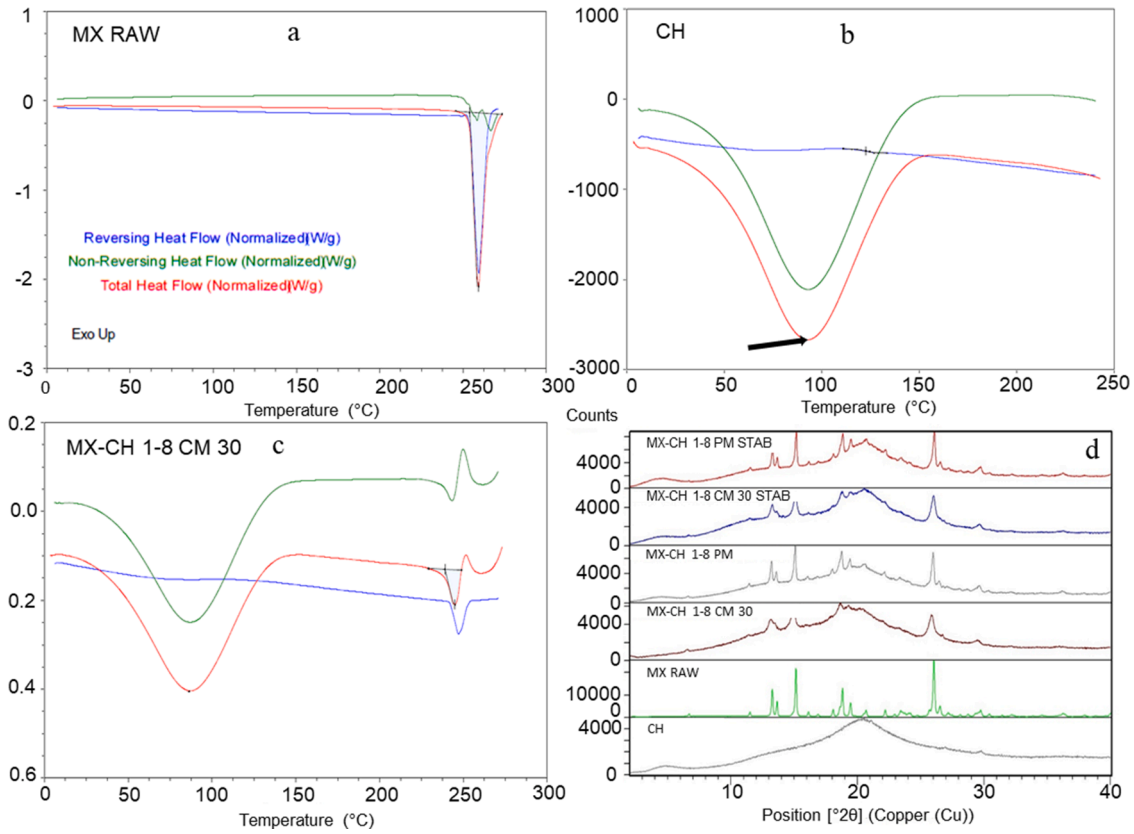

Fig. 7. a DSC thermogram of raw meloxicam, b DSC thermogram of chitosan (inserted arrow shows water in material), c DSC thermogram of MX-CH 1–8 CM 30, d XRPD patterns of raw meloxicam, chitosan, two prepared binary mixtures (MX-CH 1–8 PM and MX-CH 1–8 CM 30) and two prepared binary mixtures after stability tests (MX-CH 1–8 PM STAB and MX-CH 1–8 CM 30 STAB). Details are given in the text.

surface energy of the system was governed mainly by the surface area with smaller fluctuations due to the surface disorder caused by milling.

The net effect of the co-milling induced surface energy can be perceived by a negative linear relationship ($R^2 = 0.4449$) displaying the surface weighed dissolution rate as a function of the dispersive surface energy of the formulation:

$$\frac{r_{MAX}}{S_{TOTAL}} = -0.2644 \times \gamma^D + 15.069 \quad (4)$$

3.5. Effect of preparation method on the drug crystallinity

The mechanical energy employed in particle size reduction by milling can lead to the mechano-chemical activation of material changing its structure by defects, dislocations or strain, or to partially or totally amorphous one (Lin et al., 2010; Varghese and Ghoroi, 2017). Even though amorphization enhances the drug aqueous solubility and dissolution rate (Edueng et al., 2019; Slámová et al., 2020), this effect is temporary and while stabilization is common practice for solid dispersions, it would be much harder to stabilize drug disorder in powder mixtures (Bhende and Jadhav, 2012; Laitinen et al., 2013; Alhalaweh et al., 2015; Edueng et al., 2019).

The thermal properties of MX and CH were therefore investigated using modulated DSC; thermograms are shown in Figs. 7a and 7b, respectively. The crystalline structure of MX was characterized by a melting endotherm at 255.2 °C, the heat of fusion was 172.1 J/g. In contrast, amorphous CH was characterized by a glass transition temperature T_g of 122.5 °C; the amount of water (inserted arrow in Fig. 7b) of approximately 7% (w/w) was determined by the thermogravimetric analysis. No effect on melting point (T_{mp}) was observed for MX blank CM

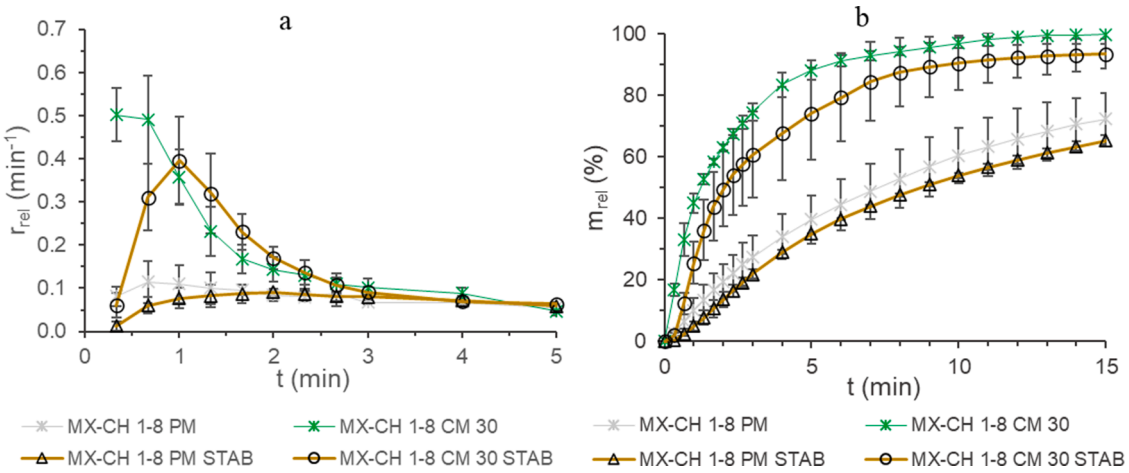

Fig. 8. Stability study of selected binary mixtures (a Relative dissolution rate of meloxicam, b Relative amount of released meloxicam after 15 min). Details are given in the text.

15 by activation due to 15 min of milling. XRPD diffractograms of raw MX and CH are depicted in Fig. 7d. MX RAW is expressed by sharp and highly intense diffraction peaks corresponding to MX polymorphic form I (Coppi et al., 2005); amorphous CH was characterized by a broaden halo.

In order to detect undesirable changes in crystalline structure of MX brought about the preparation procedure used, all binary mixtures were evaluated by MDSC as well. No changes in crystalline structure were observed. The results of MX melting temperature are summarized in Table S1 (Supplementary Material) and show the crystal form; the values of the heat of fusion were influenced only by the decrease in MX content in the mixtures for different MX-CH ratios. The results are also illustrated in MX-CH 1–8 CM 30 thermogram (Fig. 7c), representing the sample with the longer co-milling. In Fig. 7d, minimum changes were also noted in diffractograms as shown for the MX-CH 1–8 PM physical mixture as well as the MX-CH 1–8 CM 30 co-milled one. The small decrease in intensity and slightly different shape of peaks in latter were attributed to the micronization of the drug particles. Thus, no marked formation of amorphous MX was observed.

3.6. Stability studies

Adequate drug stability is targeted in the development of pharmaceutical dosage forms. Therefore, the stability study at 40 °C and 75% relative air humidity (RH) was finally performed for the most promising MX-CH 1–8 PM and MX-CH 1–8 CM 30 mixtures. After 1 month of storage in an open container, the samples were analyzed by dissolution test, MDSC and XRPD. The crystalline form of the drug remained stable (Fig. 7d, samples STAB) showing no significant changes of the heat of fusion (Table S1 in Supplementary Material); only slightly lower values of r_{rel} in the first minute of drug dissolution (Fig. 8a) were observed. As shown in Fig. 8b, the relative amount of dissolved drug reached still more than 90% of the values detected in the case of freshly prepared samples. However, the stability of the obtained mixtures would have to be studied further.

4. Conclusion

Many methods are commonly used to improve the aqueous dissolution rate of the BCS II drugs. In this mechanistic study, binary interactive mixtures of a model drug, MX, with the polysaccharide excipient CH were prepared by mixing and co-milling method, respectively, using three different drug/excipient mass ratios 1–1, 1–4, and 1–8. In comparison with the raw MX as well as the one activated by mixing and milling for 15 min, respectively, the results confirmed that the CH addition increased the dissolution rate of the BCS II drug MX in both technological procedures used. The effect of CH on the MX r_{rel} was ratio-dependent with the highest m_{rel} in the MX-CH 1–8 ratio. The effect was particularly visible within the first five minutes after contact of a powder sample with the liquid medium. The highest MX r_{MAX} 0.50 min^{-1} was detected for MX-CH 1–8 co-milled for 30 min which was five times higher comparing with the corresponding physical mixture (mixed only) and fifty times higher comparing with the raw MX.

The correlation analysis confirmed the strong CH effect on MX release as the r_{MAX} was proportional to the total surface area of the interactive mixtures prepared, rather than the portion of the surface area corresponding to MX only. This observation results in the formulation ability to control the dissolution rate by both the MX-CH ratio and the particle size distribution, which is valuable for the design of the final solid dosage form.

Finally, no marked amorphization of the drug after milling was detected by using modulated DSC and XRPD techniques. IGC was found to be highly valuable within the scope of the study Thus, the balance of cohesive and adhesive interparticle forces in interactive MX-CH mixtures was expressed by the work of adhesion/cohesion ratio of 0.9, which showed the preferential bonds of MX to the coarse particles of CH. This encourages the conclusion about the effective formation and promising stability of interactive mixtures without generally observed problems such as particle segregation or agglomeration. The goal to achieve interactive mixtures without noticeable amorphization could be a pertinent approach with respect to BCS class II drugs and even though this approach would require advanced analytics in development, it is straightforward from a manufacturing viewpoint. In addition, the analysis of surface energy change suggests the promising ability of CH to form interactive mixtures also with other drugs having similar surface properties as MX. However, such generalization needs future study.

CRediT authorship contribution statement

Jana Brokešová: Methodology, Investigation, Visualization, Data curation, Writing – original draft. **Michaela Slámová:** Investigation, Resources. **Petr Zámostný:** Conceptualization, Methodology, Writing – review & editing. **Martin Kuentz:** Conceptualization, Methodology, Writing – review & editing. **Jakub Koktan:** Supervision, Writing – review & editing. **Lukáš Krejčík:** Investigation, Visualization. **Barbora Vraníková:** Visualization, Writing – review & editing. **Petra Svačinová:** Investigation. **Zdenka Šklubalová:** Conceptualization, Methodology, Supervision, Writing – review & editing.

Declaration of Competing Interest

The authors declare that they have no conflict of interest.

Acknowledgments

This study was supported by the Charles University Grant Agency [Grant Nos. 268120/2020, SVV 260 547] and by The Parc. The authors would like to acknowledge Mgr. Ondřej Dammer, Ph.D. for cooperation with XRPD analysis.

Supplementary materials

Supplementary material associated with this article can be found, in the online version, at doi:10.1016/j.ejps.2021.106087.

References

Alhalaweh, A., Alzghoul, A., Mahlin, D., Bergström, C.A.S., 2015. Physical stability of drugs after storage above and below the glass transition temperature: relationship to glass-forming ability. Int. J. Pharm. 495 (1), 312–317. https://doi.org/10.1016/j.ijpharm.2015.08.101.

Al-Kassas, R., Bansal, M., Shaw, J., 2017. Nanosizing techniques for improving bioavailability of drugs. J. Control. Release 260, 202–212. https://doi.org/10.1016/j.jconrel.2017.06.003.

Allahham, A., Maswadeh, H.M., 2014. Study of dissolution kinetics for poorly water-soluble drugs from ternary interactive mixtures in comparison with commercially available capsules. J. Pharm. Innov. 9, 106–114. https://doi.org/10.1007/s12247-014-9177-2.

Amidon, G.L., Lennernäs, H., Shah, V.P., Crison, J.R., 1995. A theoretical basis for a biopharmaceutic drug classification: the correlation of *in vitro* drug product dissolution and *in vivo* bioavailability. Pharm. Res. 12 (3), 413–420. https://doi.org/10.1023/a:1016212804288.

Azofeifa, D.E., Arguedas, H.J., Vargas, W.E., 2012. Optical properties of chitin and chitosan biopolymers with application to structural color analysis. Opt. Mater. 35 (2), 175–183. https://doi.org/10.1016/j.optmat.2012.07.024.

Badwan, A.A., Rashid, I., Al Omari, M.M.H., Darras, F.H., 2015. Chitin and chitosan as direct compression excipients in pharmaceutical applications. Mar. Drugs 13 (3), 1519–1547. https://doi.org/10.3390/md13031519.

Bartos, C., Ambrus, R., Kovács, A., Gáspár, R., Sztojkov-Ivanov, A., Márki, Á., Janáky, T., Tömösi, F., Kecskeméti, G., Szabó-Révész, P., 2018. Investigation of absorption routes of meloxicam and its salt form from intranasal delivery systems. Molecules 23 (4), 784. https://doi.org/10.3390/molecules23040784.

Beyssac, E., Lavigne, J., 2005. Dissolution study of active pharmaceutical ingredients using the flow through apparatus USP 4. Dissolution Technol. 12 (2), 23–25. https://doi.org/10.14227/DT120205P23.

Bhende, S., Jadhav, N., 2012. Moringa coagulant as a stabilizer for amorphous solids: part I. AAPS PhamSciTech 13 (2), 400–410. https://doi.org/10.1208/s12249-012-9755-x.

Bolourchian, N., Talamkhani, Z., Nokhodchi, A., 2019. Preparation and physicochemical characterization of binary and ternary ground mixtures of carvedilol with PVP and SLS aimed to improve the drug dissolution. Pharm. Dev. Technol. 24 (9), 1115–1124. https://doi.org/10.1080/10837450.2019.1641516.

Bunker, M., Zhang, J., Blanchard, R., Roberts, C.J., 2011. Characterising the surface adhesive behavior of tablet tooling components by atomic force microscopy. Drug Dev. Ind. Pharm. 37 (8), 875–885. https://doi.org/10.3109/03639045.2010.546402.

Capece, M., Ho, R., Strong, J., Gao, P., 2015. Prediction of powder flow performance using a multi-component granular bond number. Powder Technol. 286, 561–571. https://doi.org/10.1016/j.powtec.2015.08.031.

Capece, M., Silva, K.R., Sunkara, D., Strong, J., Gao, P., 2016. On the relationship of inter-particle cohesiveness and bulk powder behavior: flowability of pharmaceutical powders. Int. J. Pharm. 511 (1), 178–189. https://doi.org/10.1016/j.ijpharm.2016.06.059.

Coppi, L., Sanmarti, M.B., Clavo, M.C., (2005), Crystalline forms of meloxicam and processes for their preparation and interconversion, U.S. Patent No 6,967,248. https://patentimages.storage.googleapis.com/64/ec/be/b9f9a7f2dd59f2/US6967248.pdf.

De Kruif, J.K., Khoo, J., Bravo, R., Kuentz, M., 2013. Novel quality by design tools for concentrated drug suspensions: surface energy profiling and the fractal concept of flocculation. J. Pharm. Sci. 102 (3), 994–1007. https://doi.org/10.1002/jps.23435.

Dhakar, N.K., Caldera, F., Bessone, F., Cecone, C., Pedrazzo, A.R., Cavalli, R., Dianzani, C., Trotta, F., 2019. Evaluation of solubility enhancement, antioxidant activity, and cytotoxicity studies of kynurenic acid loaded cyclodextrin nanosponge. Carbohydr. Polym. 224, 115168 https://doi.org/10.1016/j.carbpol.2019.115168.

Dutta, P.K., Dutta, J., Tripathi, V.S., 2004. Chitin and chitosan: chemistry, properties and applications. J. Sci. Ind. Res. 63 (1), 20–31. https://doi.org/10.1016/j.foodhyd.2010.08.008.

Edueng, K., Bergstörm, C.A.S., Gråsjö, J., Mahlin, D., 2019. Long-term physical (in) stability of spray-dried amorphous drugs: relationship with glass-forming ability and physicochemical properties. Pharmaceutics 11 (9), 425. https://doi.org/10.3390/pharmaceutics11090425.

Fowkes, F.M., 1964. Attractive forces at interfaces. Ind. Eng. Chem. 56 (12), 40–52. https://doi.org/10.1021/ie50660a008.

Freitas, J.T.J., Viana, O.M.M.S., Bonfilio, R., Doriguetto, A.C., de Araújo, M.B., 2017. Analysis of polymorphic contamination in meloxicam raw materials and its effects on the physicochemical quality of drug product. Eur. J. Pharm. Sci. 109, 347–358. https://doi.org/10.1016/j.ejps.2017.08.029.

Garg, U., Chauhan, S., Nagaich, U., Jain, N., 2019. Current advances in chitosan nanoparticles based drug delivery and targeting. Adv. Pharm. Bull. 9 (2), 195–204. https://doi.org/10.15171/apb.2019.023.

Hagen, E., Løding, F.S., Mattsson, S., Tho, I., 2016. Use of interactive mixtures to obtain mini-tablets with high dose homogeneity for paediatric drug delivery. J. Drug Deliv. Sci. Technol. 34, 51–59. https://doi.org/10.1016/j.jddst.2016.03.006.

Hamishehkar, H., Emami, S., Lamei, B., Valizadeh, H., Jouyban, A., 2014. Evaluation of solubility and dissolution profile of itraconazole after cogrinding with various hydrophilic carriers. J. Drug Deliv. Sci. Technol. 24 (6), 653–658. https://doi.org/10.1016/S1773-2247(14)50132-3.

Han, H.K., Choi, H.K., 2007. Improved absorption of meloxicam via salt formation with ethanolamines. Eur. J. Pharm. Biopharm. 65 (1), 99–103. https://doi.org/10.1016/j.ejpb.2006.07.003.

Hooton, J.C., Jones, M.D., Price, R., 2006. Predicting the behavior of novel sugar carriers for dry powder inhaler formulations via the use of a cohesive-adhesive force balance approach. J. Pharm. Sci. 95 (6), 1288–1297. https://doi.org/10.1002/jps.20618.

Horváth, T., Ambrus, R., Völgyi, G., Budai-Szűcs, M., Márki, A., Sipos, P., Bartos, C., Seres, A.B., Sztojkov-Ivanov, A., Takács-Novák, K., Csányi, E., Gáspár, R., Szabó-Révész, P., 2016. Effect of solubility enhancement on nasal absorption of meloxicam. Eur. J. Pharm. Sci. 95, 96–102. https://doi.org/10.1016/j.ejps.2016.05.031.

Huang, Y., Huang, Z., Zhang, X., Zhao, Z., Zhang, X., Wang, K., Ma, C., Zhu, C., Pan, X., Wu, C., 2018. Chitosan-based binary dry powder inhaler carrier with nanometer roughness for improving *in vitro* and *in vivo* aerosolization performance. Drug Deliv. Transl. Res. 8, 1274–1288. https://doi.org/10.1007/s13346-018-0564-y.

Hussain, A., Smith, G., Khan, K.A., Bukhari, N.I., Pedge, N.I., Ermolina, I., 2018. Solubility and dissolution rate enhancement of ibuprofen by co-milling with polymeric excipients. Eur. J. Pharm. Sci. 123, 395–403. https://doi.org/10.1016/j.ejps.2018.08.001.

Jirát, J., Zvoníček, V., Babor, M., Ridvan, L., Skořepová, E., Dušek, M., Šoóš, M., 2020. Formation of the first non-isostructural cocrystal of apremilast explained. Cryst. Growth Des. 20 (9), 5785–5795. https://doi.org/10.1021/acs.cgd.0c00393.

Karde, V., Guo, M., Heng, J.Y.Y., 2020. Influence of interparticle structuring on the surface energetics of a binary powder system. Int. J. Pharm. 581, 119295 https://doi.org/10.1016/j.ijpharm.2020.119295.

Khan, A.D., Singh, L., 2016. Various techniques of bioavailability enhancement: a review. J. Drug Deliv. Ther. 6 (3), 34–41. https://doi.org/10.22270/jddt.v6i3.1228.

Kuncahyo, I., Choiri, S., 2015. The influence of magnesium stearate, purified talc and combination of both on ternary/quaternary interactive mixture of freely and poorly water-soluble drug. Int. J. Pharm. Pharm. Sci. 7 (1), 397–402. https://innovareacademics.in/journals/index.php/ijpps/article/view/3564.

Kulvanich, P., Stewart, P.J., 1987. Fundamental considerations in the measurement of adhesional forces between particles using the centrifuge method. Int. J. Pharm. 35 (1–2), 111–120. https://doi.org/10.1016/0378-5173(87)90079-2.

Lai, F., Hersey, J.A., Staniforth, J.N., 1981. Segregation and mixing of fine particles in an ordered mixture. Powder Technol. 28 (1), 17–23. https://doi.org/10.1016/0032-5910(81)87004-0.

Laitinen, R., Löbmann, K., Strachan, C.J., Grohganz, H., Rades, T., 2013. Emerging trends in the stabilization of amorphous drugs. Int. J. Pharm. 453 (1), 65–79. https://doi.org/10.1016/j.ijpharm.2012.04.066.

Li, J., Yang, Y., Zhao, M., Xu, H., Ma, J., Wang, S., 2017. Improved oral bioavailability of probucol by dry media-milling. Mater. Sci. Eng. C 78, 780–786. https://doi.org/10.1016/j.msec.2017.04.141.

Li, Y., Yu, J., Hu, S., Chen, Z., Sacchetti, M., Sun, C.C., Yu, L., 2019. Polymer nanocoating of amorphous drugs for improving stability, dissolution, powder flow, and tabletability: the case of chitosan-coated indomethacin. Mol. Pharm. 16 (3), 1305–1311. https://doi.org/10.1021/acs.molpharmaceut.8b01237.

Lin, S.Y., Hsu, C.H., Ke, W.T., 2010. Solid-state transformation of different gabapentin polymorphs upon milling and co-milling. Int. J. Pharm. 396 (1–2), 83–90. https://doi.org/10.1016/j.ijpharm.2010.06.014.

Lipinski, C.A., 2000. Drug-like properties and the causes of poor solubility and poor permeability. J. Pharmacol. Toxicol. Methods 44 (1), 235–249. https://doi.org/10.1016/S1056-8719(00)00107-6.

Liu, H., Taylor, L.S., Edgar, K.J., 2015. The role of polymers in oral bioavailability enhancement; a review. Polymer 77, 399–415. https://doi.org/10.1016/j.polymer.2015.09.026 (Guildf).

Loh, Z.H., Samanta, A.K., Heng, P.W.S., 2015. Overview of milling techniques for improving the solubility of poorly water-soluble drugs. Asian J. Pharm. Sci. 10 (4), 255–274. https://doi.org/10.1016/j.ajps.2014.12.006.

Lohrmann, M., Kappl, M., Butt, H.J., Urbanetz, N.A., Lippold, B.C., 2007. Adhesion forces in interactive mixtures for dry powder inhalers – evaluation of a new measuring method. Eur. J. Pharm. Biopharm. 67 (2), 579–586. https://doi.org/10.1016/j.ejpb.2007.02.011.

Marinko, N., Zámostný, P., 2020. Meloxicam carrier systems having enhanced release and aqueous wettability prepared using micro-suspensions in different liquid media. AAPS PharmSciTech 21, 155. https://doi.org/10.1208/s12249-020-01701-4.

Mu, H., Holm, R., Müllertz, A., 2013. Lipid-based formulations for oral administration of poorly water-soluble drugs. Int. J. Pharm. 453 (1), 215–224. https://doi.org/10.1016/j.ijpharm.2013.03.054.

Nagy, Z.K., Balogh, A., Vajna, B., Farkas, A., Patyi, G., Kramarics, Á., Marosi, G., 2012. Comparison of electrospun and extruded Soluplus®-based solid dosage forms of improved dissolution. J. Pharm. Sci. 101 (1), 322–332. https://doi.org/10.1002/jps.22731.

Nguyen, T.T., Rambanapasi, C., de Boer, A.H., Frijlink, H.W., P.M.v.D, Ven, de Vries, J., Busscher, H.J., Maarschalk, K.v.D.V., 2010. A centrifuge method to measure particle cohesion forces to substrate surfaces: the use of a force distribution concept for data interpretation. Int. J. Pharm. 393 (1–2), 88–95. https://doi.org/10.1016/j.ijpharm.2010.04.016.

Obaidat, A., Obaidat, R., 2011. Development and evaluation of fast-dissolving tablets of meloxicam-β-cyclodextrin complex prepared by direct compression. Acta Pharm. 61, 83–91. https://doi.org/10.2478/v10007-011-0005-7.

Obaidat, R., Al-Taani, B., Al-Quraan, H., 2017. Effect of selected polymers on dissolution and stabilization of amorphous form of meloxicam. Int. J. Pharm. Pharm. Sci. 9 (9), 33–42. https://doi.org/10.22159/ijpps.2017v9i9.18621.

Panayiotou, C., Mastrogeorgopoulos, S., Hatzimanikatis, V., 2017. On Lewis acidity/basicity and hydrogen bonding in the equation-of-state approach. J. Chem. Thermodyn. 110, 3–15. https://doi.org/10.1016/j.jct.2017.02.003.

Pilcer, G., Wauthoz, N., Amighi, K., 2012. Lactose characteristics and the generation of the aerosol. Adv. Drug Deliv. Rev. 64 (3), 233–256. https://doi.org/10.1016/j.addr.2011.05.003.

Podczeck, F., Newton, J.M., James, M.B., 1997. Variations in the adhesion force between a drug and carrier particles as a result of changes in the relative humidity of the air. Int. J. Pharm. 149 (2), 151–160. https://doi.org/10.1016/S0378-5173(97)04869-2.

Rasenack, N., Müller, B.W., 2004. Micron-size drug particles: common and novel micronization techniques. Pharm. Dev. Technol. 9 (1), 1–13. https://doi.org/10.1081/PDT-120027417.

Romani, L.F.A., Yoshida, M.I., Gomes, E.C.L., Machado, R.R., Rodrigues, F.F., Coelho, M. M., Oliveira, M.A., Freitas-Marques, M.B., San Gil, R.A.S., Mussel, W.N., 2018. Physicochemical characterization, the Hirshfeld surface, and biological evaluation of two meloxicam compounding pharmacy samples. J. Pharm. Anal. 8 (2), 103–108. https://doi.org/10.1016/j.jpha.2017.12.006.

Saeki, I., Kondo, K., Nagase, R., Yoshida, M., Niwa, T., 2019. Design of swellable ordered-mixed spherical drug particles (Swell-OM-spheres) using a dry powder milling and coating technique to improve dissolution behavior. J. Drug Deliv. Sci. Technol. 54, 101281 https://doi.org/10.1016/j.jddst.2019.101281.

Schultz, J., Lavielle, L., Martin, C., 1987. The role of the interface in carbon fibre-epoxy composites. J. Adhes. 23, 45–60. https://doi.org/10.1080/00218468708080469.

Shete, A.S., Yadav, A.V., Murthy, S.M., 2012. Chitosan and chitosan chlorhydrate based various approaches for enhancement of dissolution rate of carvedilol. DARU J. Pharm. Sci. 20 (1), 1–9. https://doi.org/10.1186/2008-2231-20-93.

Slámová, M., Prausová, K., Epikaridisová, J., Brokešová, J., Kuentz, M., Patera, J., Zámostný, P., 2021. Effect of co-milling on dissolution rate of poorly soluble drugs. Int. J. Pharm. 597, 120312 https://doi.org/10.1016/j.ijpharm.2021.120312.

Slámová, M., Školáková, T., Školáková, A., Patera, J., Zámostný, P., 2020. Preparation of solid dispersions with respect to the dissolution rate of active substance. J. Drug Deliv. Sci. Technol. 56, 101518 https://doi.org/10.1016/j.jddst.2020.101518.

Školáková, T., Souchová, L., Patera, J., Pultar, M., Školáková, A., Zámostný, P., 2019. Prediction of drug-polymer interactions in binary mixtures using energy balance supported by inverse gas chromatography. Eur. J. Pharm. Sci. 130, 247–259. https://doi.org/10.1016/j.ejps.2019.01.021.

Tran, D.T., Bittner, R., Zámostný, P., 2021. Adhesion force measurement by centrifuge technique as tool for predicting interactive mixture stability. Chem. Eng. Res. Des. 165, 467–476. https://doi.org/10.1016/j.cherd.2020.10.012.

Tsume, Y., Mudie, D.M., Langguth, P., Amidon, G.E., Amidon, G.L., 2014. The biopharmaceutics classification system: subclasses for *in vivo* predictive dissolution (IPD) methodology and IVIVC. Eur. J. Pharm. Sci. 57, 152–163. https://doi.org/10.1016/j.ejps.2014.01.009.

Varghese, S., Ghoroi, C., 2017. Improving the wetting and dissolution of ibuprofen using solventless co-milling. Int. J. Pharm. 533 (1), 145–155. https://doi.org/10.1016/j.ijpharm.2017.09.062.

Verreck, G., Chun, I., Peeters, J., Rosenblatt, J., Brewster, M.E., 2003. Preparation and characterization of nanofibers containing amorphous drug dispersions generated by electrostatic spinning. Pharm. Res. 20 (5), 810–817. https://doi.org/10.1023/a:1023450006281.

Vraníková, B., Niederquell, A., Ditzinger, F., Šklubalová, Z., Kuentz, M., 2020. Mechanistic aspects of drug loading in liquisolid systems with hydrophilic lipid-based mixtures. Int. J. Pharm. 578, 119099 https://doi.org/10.1016/j.ijpharm.2020.119099.

Wang, H., George, G., Islam, N., 2018. Nicotine-loaded chitosan nanoparticles for dry powder inhaler (DPI) formulations – impact of nanoparticle surface charge on powder aerosolization. Adv. Powder Technol. 29 (12), 3079–3086. https://doi.org/10.1016/j.apt.2018.08.011.

Yang, C., Xu, X., Wang, J., An, Z., 2012. Use of the co-grinding method to enhance the dissolution behavior of a poorly water-soluble drug: generation of solvent-free drug-polymer solid dispersions. Chem. Pharm. Bull. 60 (7), 837–845. https://doi.org/10.1248/cpb.c12-00034.

Yu, D.G., Zhang, X.F., Shen, X.X., Brandford-White, C., Zhu, L.M., 2009. Ultrafine ibuprofen-loaded polyvinylpyrrolidone fiber mats using electrospinning. Polym. Int. 58 (9), 1010–1013. https://doi.org/10.1002/pi.2629.

Zhou, Q.T., Morton, D.A.V., 2012. Drug–lactose binding aspects in adhesive mixtures: controlling performance in dry powder inhaler formulations by altering lactose carrier surfaces. Adv. Drug Del. Rev. 64 (3), 275–284. https://doi.org/10.1016/j.addr.2011.07.002.